ISSN 1560-3547, Regular and Chaotic Dynamics, 2022, Vol. 27, No. 2, pp. 198–216. © Pleiades Publishing, Ltd., 2022.

On 1:3 Resonance Under Reversible Perturbations of Conservative Cubic Hénon Maps

Marina S. Gonchenko[1*], Alexey O. Kazakov[2], Evgeniya A. Samylina[2,3***], and Aikan Shykhmamedov[2****]**

[1] *Universitat de Barcelona, Gran Via de les Corts Catalanes, 585, 08007 Barcelona, Spain*

[2] *National Research University Higher School of Economics, ul. Bolshaya Pecherskaya 25/12, 603155 Nizhny Novgorod, Russia*

[3] *Lobachevsky State University of Nizhny Novgorod, pr. Gagarina 23, 603950 Nizhny Novgorod, Russia*

Received October 22, 2021; revised January 27, 2022; accepted February 16, 2022

Abstract—We consider reversible nonconservative perturbations of the conservative cubic Hénon maps $H_3^{\pm} : \bar{x} = y, \bar{y} = -x + M_1 + M_2 y \pm y^3$ and study their influence on the 1:3 resonance, i. e., bifurcations of fixed points with eigenvalues $e^{\pm i2\pi/3}$. It follows from [1] that this resonance is degenerate for $M_1 = 0, M_2 = -1$ when the corresponding fixed point is elliptic. We show that bifurcations of this point under reversible perturbations give rise to four 3-periodic orbits, two of them are symmetric and conservative (saddles in the case of map H_3^+ and elliptic orbits in the case of map H_3^-), the other two orbits are nonsymmetric and they compose symmetric couples of dissipative orbits (attracting and repelling orbits in the case of map H_3^+ and saddles with the Jacobians less than 1 and greater than 1 in the case of map H_3^-). We show that these local symmetry-breaking bifurcations can lead to mixed dynamics due to accompanying global reversible bifurcations of symmetric nontransversal homo- and heteroclinic cycles. We also generalize the results of [1] to the case of the $p : q$ resonances with odd q and show that all of them are also degenerate for the maps $H_3^{\pm}$ with $M_1 = 0$.

MSC2010 numbers: 37G25, 37G35

DOI: 10.1134/S1560354722020058

Keywords: cubic Hénon map, reversible system, 1:3 resonance, homoclinic tangencies, mixed dynamics.

1. INTRODUCTION

In the present paper we study how reversible nonconservative perturbations affect the 1:3 resonance, i.e., bifurcations of fixed points with eigenvalues $e^{\pm i2\pi/3}$, in conservative cubic Hénon maps of the form

$$H_3^{\pm} : \ (x, y) \to (\bar{x}, \bar{y}) \ : \bar{x} = y, \quad \bar{y} = -x + M_1 + M_2 y \pm y^3, \tag{1.1}$$

where x and y are coordinates, and M_1 and M_2 are parameters. This problem has become very interesting due to the recent discovery of *mixed dynamics* [2, 3], a third, new type of dynamical chaos.

Recall that mixed dynamics is such type of chaotic behavior of orbits for which chaotic attractors and repellers intersect but do not coincide [3]. This type of chaos is a complement to other two

*E-mail: gonchenko@ub.edu

**E-mail: kazakovdz@yandex.ru

***E-mail: samylina_evgeniya@mail.ru

****E-mail: aykhansh@gmail.com

well-known types of chaotic behavior for systems with compact phase space: the dissipative chaos, when an attractor is separated from a repeller, and the conservative (e.g., Hamiltonian) chaos for which the whole phase space is the attractor and repeller simultaneously. Note that mixed dynamics often appear in applications: the nonholonomic models of the Celtic stone and the Chaplygin top were the first systems where it was purposefully found [4, 5], now many systems are known which exhibit mixed dynamics, see, e. g., [6–17]. In all these studies two sides of the mixed dynamics phenomenon are taken into account: first, to detect it, i. e., to show numerically or experimentally that attractors and repellers visually intersect, and, second, to prove mathematically that they indeed have nonempty intersection, using known criteria of mixed dynamics [18–21]. As far as we know, both these approaches were combined only in a couple of papers, see, e. g., [6, 22, 23]. The second approach (to prove) is much more delicate than the first one, it requires involving various theoretical aspects of mixed dynamics such as criteria for the existence of absolute Newhouse regions[1)] [18–21, 24] and the structure of bifurcation scenarios leading to the appearance of mixed dynamics, see, e. g., [6, 10, 22]. In the present paper, we apply both these approaches when studying local and global bifurcations associated with the 1:3 resonance under reversible perturbations of the cubic Hénon maps.

It is also important to note that the cubic Hénon maps (1.1) are interesting not only in their own right, as the simplest nonlinear maps demonstrating complicated dynamics, but also as normal forms of first-return maps near cubic homoclinic tangencies in area-preserving diffeomorphisms [26]. Note that the different signs $\pm$ before the cubic term y^3 correspond to two different types of cubic homoclinic tangencies, see [26–28] for more details. In the case of reversible maps, it is well known that the appearance of such symmetric homoclinic tangencies is a codimension one bifurcation phenomenon which, in turn, implies the existence of Newhouse domains in which homoclinic tangencies, including symmetric cubic homoclinic tangencies, are dense [21]. Then their bifurcations leading to the emergence of symmetric pairs of nonconservative periodic orbits provide a criterion of reversible mixed dynamics [20]. Namely, in the corresponding absolute Newhouse domains, reversible maps with infinitely many periodic sinks (stable or attracting orbits), sources (completely unstable or repelling orbits), saddles with the Jacobian greater than 1, and saddles with the Jacobian less than 1, as well as symmetric elliptic periodic orbits and conservative saddles, are dense.

It is widely known that the strong 1:1, 1:2, 1:3 and 1:4 resonances, i. e., bifurcations of fixed points (periodic orbits) with eigenvalues $e^{\pm 2\pi i/q}$, $q = 1, 2, 3, 4$, respectively, are very important for dynamics. In the conservative setting, the nondegenerate 1:1 resonance is related to a parabolic (elliptic-hyperbolic) bifurcation of fixed (periodic) points that implies the appearance of a pair of saddle and elliptic orbits. In turn, the nondegenerate 1:2 resonance is connected with a conservative period-doubling bifurcation. The 1:3 and 1:4 resonances are most difficult, their theory was outlined by V. Arnold in [29], where, in particular, a case of the degenerate 1:4 resonance (the so-called "Arnold degeneracy") was considered, see also [30]. As is well known, the complex local normal form of an area-preserving map near a fixed point with eigenvalues $\pm i$ (1:4 resonance) is written as $\bar{z} = i(z + A|z|^2 z + B(z^*)^3) + O(|z|^5)$, where A and B are real coefficients. The Arnold degeneracy corresponds to the case $|A| = |B|$. It is very interesting that recently, in [26, 31], a new type of degenerate resonance $1 : 4$ has been found. It corresponds to the case $B = 0$. This degeneracy is very interesting since its two-parameter unfolding includes symmetry-breaking (pitchfork) bifurcations of 4-periodic orbits.

Note that a class of degenerate $p : q$ resonances accompanied by symmetry-breaking bifurcations of q-periodic points was described in [32]. The 1:4 resonance fits well into this class [26], while the 1:3 degenerated resonances have certain peculiarities, which were not considered in [32]. In this paper we deal with this problem. We note, in particular, that degenerated resonances, including the 1:3 resonance, appear in maps (1.1) at $M_1 = 0$. In this case, maps (1.1) possess the central symmetry $(x \to -x, y \to -y)$, which implies automatically that all $p : q$ resonant fixed points $O(0, 0)$ with odd

[1)] Recall that Newhouse regions are open (in C^2-topology) regions in the space of dynamical systems where systems with homoclinic tangencies are dense [25]. In absolute Newhouse regions systems with infinitely many hyperbolic periodic orbits of all types (allowed by the dimension of the phase space) are dense.

$q \geqslant 3$ are degenerate (this is a consequence of the fact that all coefficients vanish before monomials $z^n(z^*)^m$ with even $m+n$ in the corresponding normal forms), see Section 4.

The strong resonances often appear in area-preserving maps. For example, in the conservative (quadratic) Hénon map $\bar{x} = y, \bar{y} = M - x - y^2$ the structure of the 1:4 resonance was studied in [33], where it was shown that this resonance is degenerate (the Arnold case). In [33] it was also shown that, in the conservative Hénon map, the 1:3 resonance is nondegenerate, and it mainly relates to the rearrangement of symmetric 3-periodic saddle orbits. Besides, in particular, in [34] it was demonstrated that the emergence of a fixed point with eigenvalues $e^{\pm i2\pi/3}$ in the Hénon map implies both local instability of the fixed point and global instability of the map, i.e., the fixed point becomes a saddle with 6 separatrices (local effect) and almost all orbits close to the fixed point go to infinity (global effect). However, this is not the case when the 1:3 resonance is degenerate. Here, in general, the fixed point is surrounded by a garland (a chain of stability islands) which consists of elliptic and saddle 3-periodic orbits and does not allow orbits to pass far away from the fixed point. This local stability also implies global stability when the 1:3 resonance is near-degenerate. Note that such a situation takes place in the conservative cubic Hénon maps (1.1), see Section 3 (Figs. 3 and 4). Here a degenerate 1:3 resonance appears at $M_1 = 0$ and $M_2 = -1$, otherwise it is nondegenerate if $M_1 \neq 0$. We also note that all $p:q$ resonances with odd q have the same nature: they are degenerate for $M_1 = 0$ and the corresponding value of M_2, see Section 4 (Fig. 5 for the 1:5 and 1:7 resonances).

Our main goal is to study the near-degenerate 1:3 resonances in maps (1.1) and analyze how they bifurcate under reversible nonconservative perturbations. It follows from [1] that, for $M_1 = 0$ and $M_2 = -1$, the 1:3 resonance is degenerate for the conservative cubic Hénon maps and 3-periodic orbits undergo pitchfork bifurcations. We note that both maps H_3^+ and H_3^- are conservative and reversible with respect to the involution $h : (x, y) \to (y, x)$, i. e., by definition the maps $H_3^\pm$ and the inverse maps $(H_3^\pm)^{-1}$ are conjugate by means of the involution h (the relation $(H_3^\pm)^{-1} = h \circ H_3^\pm \circ h$ holds). In the general case, reversible maps can also have dissipative orbits that always exist in pairs: stable and completely unstable periodic orbits, two saddle periodic orbits with the Jacobian greater than 1 and less than 1, etc. Such orbits are symmetric to each other with respect to an involution. We call them a *symmetric couple of orbits*. When a map is reversible and conservative, symmetric couples of orbits are also conservative, however, under general reversible perturbations, these pairs become dissipative.

The genericity of perturbations means that they, first of all, should destroy the conservativity. Following the paper [35], we construct (analytically), in Section 2, such reversibility preserving perturbations for Hénon-like conservative maps, and apply them for the cubic Hénon maps (1.1), see formula (2.4). In Section 3, for the unperturbed map (1.1) we study in detail bifurcations of the conservative 1:3 resonance and mention the associated degeneracies and pitchfork bifurcations of 3-periodic orbits. Then, in Sections 5 and 6, we illustrate the bifurcation diagrams for the near-degenerate 1:3 resonance in the perturbed maps and focus on pitchfork bifurcations of 3-periodic orbits which lead to the dissipative dynamics. Namely, we demonstrate that for perturbations of H_3^+ a supercritical pitchfork bifurcation takes place with the elliptic 3-periodic orbit, which leads to the emergence of nonsymmetric attracting and repelling 3-periodic orbits, see Section 5 for more details. For the perturbed map H_3^- a subcritical pitchfork bifurcation takes place with the saddle 3-periodic orbit, which leads to the emergence of a symmetric couple of 3-periodic dissipative saddles, see Section 6. Finally, in Section 7, we provide numerical evidence of the existence of mixed dynamics in the reversible nonconservative perturbation of H_3^- and discuss possible emergence of mixed dynamics for map H_3^+.

2. CONSTRUCTION OF REVERSIBLE NONCONSERVATIVE PERTURBATIONS

In the present paper we consider two-dimensional reversible diffeomorphisms. Recall that a diffeomorphism f is reversible if it is conjugate to its inverse map f^{-1} by means of an involution h, i.e., the following relation is true: $f^{-1} = h \circ f \circ h$, where $h^2 = Id$. The property of reversibility of f implies the strong symmetry of the set of orbits. An orbit that intersects the set $Fix(R) =$

$\{x:\ R(x)=x\}$ or the set $Fix(Rf)$ is called *symmetric*. Any symmetric periodic orbit of a two-dimensional reversible orientable map has eigenvalues λ and λ^{-1}. Then it is a symmetric saddle if $0<\lambda<1$ and a symmetric elliptic point if $\lambda=e^{i\varphi}$, $\varphi\neq 0,\pi$.

As for nonsymmetric orbits, typically they are not conservative, and for any nonsymmetric orbit there exists an orbit, symmetric to it, with "opposite" dynamical properties. This means that, if a periodic orbit has eigenvalues λ_1 and λ_2, then the orbit symmetric to it has eigenvalues λ_1^{-1} and λ_2^{-1}. Nonsymmetric orbits compose a symmetric pair of orbits.

In reversible systems nonsymmetric orbits can appear via saddle-node bifurcations or due to symmetry-breaking bifurcations. Typical (codimension one) local bifurcations are supercritical and subcritical pitchfork bifurcations [36]. As a result of a supercritical bifurcation, a symmetric elliptic periodic orbit becomes a saddle and in its neighborhood a symmetric couple "sink-source" appears, see Figs. 1a, 1b. Under a subcritical bifurcation, the saddle periodic orbit becomes elliptic and there appears a symmetric pair of saddle periodic orbits, one with the Jacobian $J<1$ and the other with the Jacobian $J>1$, see Figs. 1c, 1d.[2)] It is important to note that local symmetry-breaking bifurcations can be considered as an indicator of mixed dynamics in systems where the difference between the intersecting attractor and repeller is invisible in standard numerics, for instance, as in the nonholonomic model of a rubber disk on the plane [17].

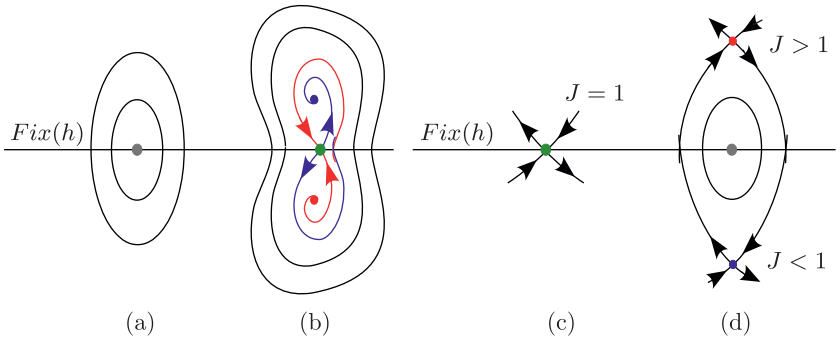

Fig. 1. Two types of reversible pitchfork bifurcation: (a)→(b) supercritical pitchfork bifurcation at which an elliptic orbit (in plot (a)) becomes a saddle orbit and a pair of stable and unstable orbits appears near the saddle (in plot (b)); (c)→(d) subcritical pitchfork bifurcation at which a saddle orbit (in plot (c)) bifurcates into an elliptic orbit surrounded by a couple of saddle orbits with the Jacobians $J>1$ and $J<1$ (in plot (d)).

Concerning global symmetry-breaking bifurcations, they are related to the appearance of nontransversal intersections between invariant manifolds of either the same periodic saddle orbit (homoclinic tangencies) or different saddles (heteroclinic tangencies). Under certain conditions bifurcations of these tangencies lead to the emergence of symmetric pairs of sinks and sources, area-expanding and area-contracting saddles as well as symmetric elliptic and saddle periodic orbits, and, hence, to the reversible mixed dynamics. Some of such global symmetry-breaking bifurcations were studied for nontransversal heteroclinic cycles of different types [18–21], see some examples of such cycles in Fig. 2.

In order to study such bifurcations in reversible maps, one needs, first of all, to construct smooth reversible perturbations that destroy their conservativity. Following the ideas of [35], we construct such perturbations for conservative generalized Hénon maps of the form

$$H:\ \bar{x}=y,\quad \bar{y}=-x+P(y), \tag{2.1}$$

where $P(y)$ is a smooth (in particular, analytical or polynomial) function of y and parameters. In particular, they include the cubic conservative Hénon maps for $P(y)=M_1+M_2y\pm y^3$.

[2)] Supercritical and subcritical pitchfork bifurcations are also typical (codimension one) local bifurcations in the conservative reversible case. Due to the supercritical pitchfork bifurcation a symmetric elliptic periodic orbit becomes a saddle orbit and a symmetric pair of elliptic periodic orbits is born in its neighborhood. Due to the subcritical pitchfork bifurcation a symmetric saddle periodic orbit becomes an elliptic one and a symmetric pair of conservative saddle (with the Jacobian $J=1$) periodic orbits is born in its neighborhood.

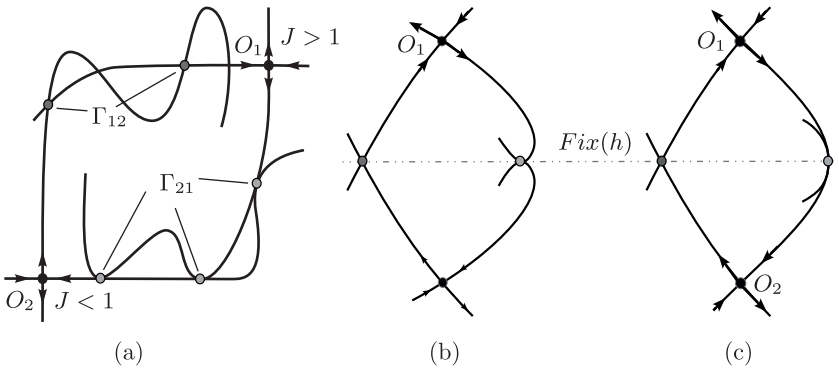

Fig. 2. Examples of nontransversal heteroclinic cycles of planar diffeomorphisms: (a) the heteroclinic cycle studied in [18]; (b) the nontransversal heteroclinic cycle with a quadratic tangency from [19]; (c) the nontransversal heteroclinic cycle with a cubic tangency from [21].

Our approach to get reversible nonconservative perturbations consists in writing the perturbations in the form

$$\tilde{H}(\varepsilon)\ :\quad \bar{x}+\varepsilon\varphi(\bar{y},\bar{x})=y+\varepsilon\varphi(x,y),\quad \bar{y}=-x+P\big(y+\varepsilon\varphi(x,y)\big), \tag{2.2}$$

where ε is a small parameter and φ is a smooth function which gives a nonconservative perturbation. This perturbation can be obtained by applying the so-called Quispel-Roberts method [37], see also [35, 38]. This method uses two facts: (i) any two-dimensional reversible map f can be presented as a composition of two involutions, $f=\zeta_1\circ\zeta_2$, and a perturbed map is obtained by perturbing one of the involutions, $\tilde{f}=\zeta_1\circ\tilde{\zeta}_2$; (ii) if ζ is an involution of map f and map T is a diffeomorphism, then $\tilde{\zeta}=T^{-1}\circ\zeta\circ T$ is also an involution of map f. Indeed, $H=h\circ h_2$, where $h:(x,y)\to(y,x)$ and $h_2:(x,y)\to(-x+P(y),y)$ are involutions. Thus, $\tilde{H}=h\circ\tilde{h}_2$ is obtained by perturbing the second involution $\tilde{h}_2=\tilde{h}_2=T^{-1}\circ h_2\circ T$ with a near-identity map $T:\ \bar{x}=x,\bar{y}=y+\varepsilon\varphi(x,y)$.

Lemma 1. *The diffeomorphism $\tilde{H}(\varepsilon)$, defined in* (2.2)*, is reversible with respect to the involution $h:(x,y)\to(y,x)$.*

Proof. The proof is similar to the one done in [20], see also [35]. Indeed, to prove the reversibility of $\tilde{H}(\varepsilon)$, we have to show that $\tilde{H}(\varepsilon)^{-1}=h\circ\tilde{H}(\varepsilon)\circ h$.

First, we write the inverse map $\tilde{H}(\varepsilon)^{-1}$ swapping the bar and no-bar variables $\bar{x}\leftrightarrow x,\bar{y}\leftrightarrow y$:

$$\tilde{H}(\varepsilon)^{-1}\ :\quad \bar{x}=-y+P\big(x+\varepsilon\varphi(y,x)\big),\quad \bar{y}+\varepsilon\varphi(\bar{x},\bar{y})=x+\varepsilon\varphi(y,x). \tag{2.3}$$

Second, the composition $\tilde{H}(\varepsilon)\circ h$ is obtained by interchanging the variables $x\to y$, $y\to x$ in $\tilde{H}(\varepsilon)$ according to the involution h

$$\tilde{H}(\varepsilon)\circ h\ :\quad \bar{x}+\varepsilon\varphi(\bar{y},\bar{x})=x+\varepsilon\varphi(y,x),\quad \bar{y}=-y+P(x+\varepsilon\varphi(y,x)).$$

Then we apply h onto $\tilde{H}(\varepsilon)\circ h$ swapping the bar variables $\bar{x}\to\bar{y}$, $\bar{y}\to\bar{x}$ and get $h\circ\tilde{H}(\varepsilon)\circ h$ which coincides with $\tilde{H}(\varepsilon)^{-1}$ in (2.3). □

For $\varepsilon=0$, map (2.2) coincides with the conservative map (2.1). We consider $P(y)=M_1+M_2y\pm y^3$ and the concrete perturbation $\varphi(x,y)=xy$:

$$\tilde{H}_3^{\pm}(\varepsilon)\ :\quad \bar{x}+\varepsilon\bar{x}\bar{y}=y+\varepsilon xy,\quad \bar{y}=-x+M_1+M_2(y+\varepsilon xy)\pm(y+\varepsilon xy)^3. \tag{2.4}$$

Since we choose a perturbation linear in the first variable x, the equations in (2.4) can be solved for $\bar{x}$ and $\bar{y}$. Thus, the maps $\tilde{H}_3^{\pm}$ can be written in the explicit form. The Jacobian of the maps equals

$$J=\frac{1+\varepsilon x}{1+\varepsilon\bar{y}},$$

which is different from 1 when $\varepsilon \neq 0$. We analyze numerically bifurcations of the 1:3 resonance in perturbed cubic conservative Hénon maps $\tilde{H}_3^{\pm}(\varepsilon)$ for $\varepsilon \neq 0$ and construct the corresponding bifurcation diagrams in Sections 5 and 6, paying special attention to the appearance of nonsymmetric periodic orbits under reversible pitchfork bifurcations.

Remark 1. Maps (2.4) are not diffeomorphisms in the whole plane $\mathbf{R^2}$. However, these maps are diffeomorphisms in a sufficiently large part of it: $D_\varepsilon : |x| < \varepsilon^{-1}, |y| < \varepsilon^{-1}$. Therefore, the question of the properties of reversible dynamics in map (2.4) at small ε is quite interesting.

We also note that for small ε the dynamics of the perturbed maps (2.4) and the initial cubic maps (1.1) are concentrated in a certain neighborhood of the origin of the phase plane, and we are not interested in what happens outside this neighborhood.

3. 1:3 RESONANCE FOR THE UNPERTURBED MAPS $H_3^{\pm}$

In the general nonconservative setting, the analysis of the 1:3 resonance was done by Arnold [29], see also [30, 39]. For the study of the 1:3 resonance in conservative maps we refer the reader to [34, 40]. Recall that one can study the structure of such bifurcations by writing the local normal form expressed in complex coordinates $z = x + iy$ and $z^* = x - iy$:

$$\bar{z} = e^{i2\pi/3}(z + a_{02}(z^*)^2 + a_{21}z^2z^*) + O(|z|^4), \tag{3.1}$$

where the coefficient a_{02} is purely imaginary since map (3.1) is reversible with respect to the involution $h : z \to z^*$. In this case the 1:3 resonance is degenerate when $a_{02} = 0$.

Let $d = \pm 1$ be the coefficient before the cubic term in (1.1), thus, $d = 1$ corresponds to H_3^+ and $d = -1$ stands for H_3^-. Then, for the parameters M_1 and M_2 on the 1:3 resonance curve

$$l_{1:3}^d : M_1^2 = \frac{d}{27}(1 + M_2)(2M_2 - 7)^2, \tag{3.2}$$

map H_3^d has the fixed point with eigenvalues $e^{\pm i2\pi/3}$ which is $P_{1:3}^{(1)} = \sqrt{-d(1 + M_2)/3}\,(1, 1)$ in the branch $M_1 > 0$ and $P_{1:3}^{(2)} = -\sqrt{-d(1 + M_2)/3}\,(1, 1)$ in the branch $M_1 < 0$. Note that the curve $l_{1:3}^-$ has a self-intersection point at $(M_1, M_2) = (0, 7/2)$ where map H_3^- has two fixed points $P_{1:3}^{(1)} = \left(\sqrt{3/2}, \sqrt{3/2}\right)$ and $P_{1:3}^{(2)} = \left(-\sqrt{3/2}, -\sqrt{3/2}\right)$ with eigenvalues $e^{\pm i2\pi/3}$ simultaneously.

The coefficients of the normal form (3.1) are as follows:

$$\begin{aligned} a_{02} &= -2i\sqrt{-d(1 + M_2)}, && \text{for } M_1 > 0, \\ a_{02} &= 2i\sqrt{-d(1 + M_2)}, && \text{for } M_1 < 0, \\ a_{21} &= -4d(1 + M_2) + 4\sqrt{3}dM_2 i. \end{aligned}$$

It is easy to see that a_{02} and a_{21} do not vanish simultaneously. Moreover, $a_{02} = 0$ at $M_2 = -1$, therefore the 1:3 resonance is degenerate when $M_1 = 0, M_2 = -1$.

A detailed bifurcation analysis for the conservative cubic Hénon maps $H_3^{\pm}$ was carried out in [1, 26, 31]. In particular, bifurcations of 3-periodic orbits were studied in [1], and one of the principal bifurcations were pitchfork bifurcations. For convenience, we display the corresponding bifurcation diagrams for H_3^+ and H_3^- and complement them with the related phase portraits in Figs. 3 and 4, respectively.

Let us briefly describe these figures. Besides the 1:3 resonance curve $l_{1:3}^d$, defined in (3.2), the further bifurcation curves are P_1^d, PD_1^d, P_3^d and PF_3^d. The curves P_1^d and PD_1^d, which have the equations

$$\begin{aligned} P_1^d : &\quad M_1^2 = \frac{4d}{27}(2 - M_2)^3, \\ PD_1^d : &\quad M_1^2 = -\frac{4d}{27}(2 + M_2)(4 - M_2)^2, \end{aligned}$$

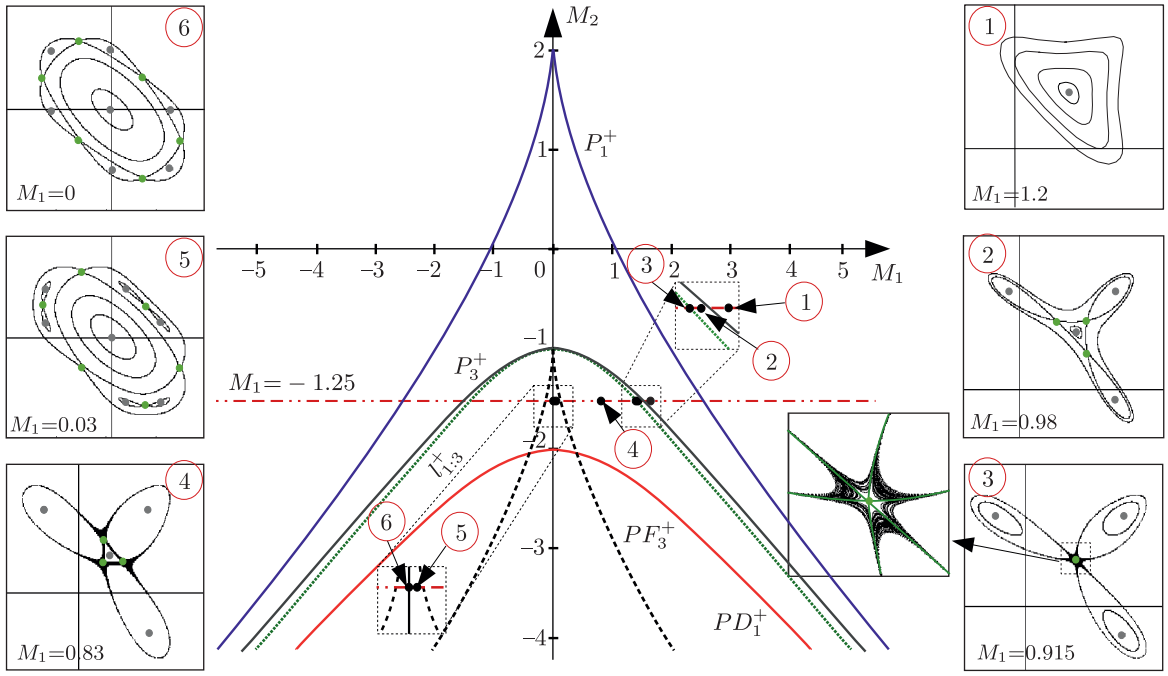

Fig. 3. Bifurcation diagram for the conservative cubic Hénon map H_3^+. The bifurcations curves P_1^+, $l_{1:3}^+$, and PD_1^+ are the curves of a parabolic (pitchfork for $M_1 = 0$) bifurcation, 1:3 resonance, and a period-doubling bifurcation of fixed points, respectively. The curves P_3^+ and PF_3^+ are the curves of parabolic and pitchfork bifurcations of 3-periodic orbits, respectively. For the fixed value of $M_2 = -1.25$, the phase portraits are presented for $M_1 = 0, 0.03, 0.83, 0.915, 0.98$ and 1.2. For $M_1 < 0$ the phase portraits are reflected symmetrically with respect to $y = -x$.

are the curves of fixed points with double eigenvalue $(1, 1)$ and $(-1, -1)$, respectively. The curve P_1^d corresponds to a parabolic bifurcation of a fixed point of map for $M_1 \neq 0, M_2 \neq 2$. As a result of this bifurcation, crossing P_1^d laterally, there appear elliptic and saddle (hyperbolic) fixed points for parameters below P_1^+ in the case of map H_3^+ and above P_1^- in the case of map H_3^-. When passing through the point $M_1 = 0, M_2 = 2$ at P_1^d vertically ($M_1 = 0$ being fixed) a subcritical and supercritical conservative pitchfork bifurcation takes place for H_3^+ and H_3^-, respectively. Namely, in the case of H_3^+, under this bifurcation the saddle fixed point for $M_2 > 2$ (above P_1^+) becomes elliptic and a pair of saddle fixed points appears around for $M_2 < 2$. For map H_3^-, passing through the point $M_1 = 0, M_2 = 2$ from bottom to top, an elliptic fixed point undergoes a supercritical pitchfork bifurcation, it turns into a saddle fixed point and a pair of elliptic fixed points appears nearby. The curve PD_1^d is related to a period-doubling bifurcation of a fixed point. At crossing PD_1^+, the elliptic fixed point becomes a saddle and in its neighborhood there appears an elliptic 2-periodic orbit. The curve PD_1^- corresponds to two different types of period-doubling bifurcation: the bottom part is responsible for a subcritical period-doubling bifurcation of the saddle fixed point (which becomes an elliptic fixed point surrounded by a saddle 2-periodic orbit), while at the upper part of PD_1^- an elliptic fixed point undergoes a supercritical period-doubling bifurcation. See [26] for more details on these bifurcations. The other curves P_3^d and PF_3^d are associated with parabolic and conservative pitchfork bifurcations of 3-periodic orbits, respectively. They were discovered by [1] and they have too cumbersome expressions to be presented, so we omit their equations.

We note that the point $(M_1, M_2) = (0, -1)$, corresponding to the case $a_{02} = 0$, is the cusp point of the curves PF_3^+ and PF_3^- in both maps H_3^+ and H_3^-, respectively. This point also lies in P_3^d and $l_{1:3}^d$. Getting inside the region bounded by the curve PF_3^+ (PF_3^-), the symmetric elliptic (saddle) 3-periodic orbit becomes a saddle (elliptic) orbit and a pair of nonsymmetric elliptic (saddle) orbits of the same period emerges for H_3^+ (H_3^-). It is worth mentioning that in the nonconservative reversible

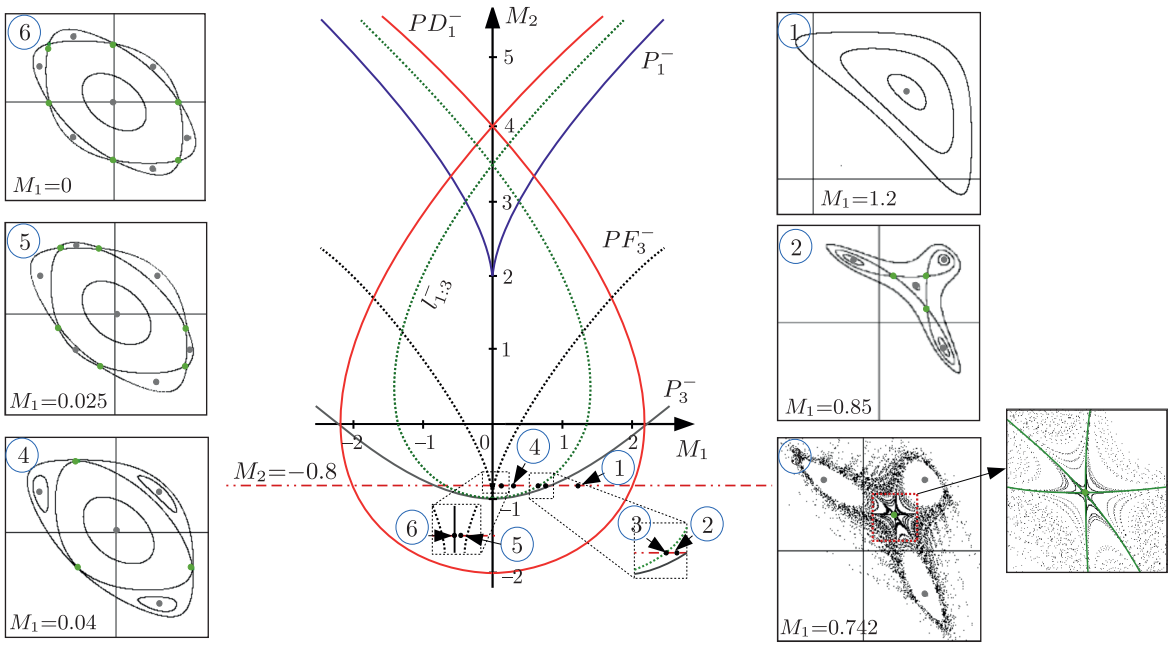

Fig. 4. Bifurcation diagram for the conservative cubic Hénon map H_3^-. The bifurcations curves P_1^-, $l_{1:3}^-$, and PD_1^- are the curves of parabolic (pitchfork for $M_1 = 0$) bifurcation, 1:3 resonance, and period-doubling bifurcation of fixed points, respectively. The curves P_3^- and PF_3^- are the curves of parabolic and pitchfork bifurcations of 3-periodic orbits, respectively. The sequence of phase portraits in the horizontal line $M_2 = -0.8$ is displayed for $M_1 = 0, 0.025, 0.04, 0.742, 0.85$, and 1.2. For $M < 0$ the phase portraits are reflected symmetrically with respect to $y = -x$.

case, instead of nonsymmetric elliptic (saddle) orbits, a pair of stable and unstable orbits (saddles with the Jacobians $J > 1$ and $J < 1$) emerges as a result of a reversible pitchfork bifurcation.

In Fig. 3 we present a sequence of phase portraits near the 1:3 resonance for a fixed M_2 for H_3^+. Let us give some details of the bifurcations which take place in the horizontal line $M_2 = -1.25$. For M_1 on the right-hand side of the right branch of P_3^+ (see the phase portrait ① for $M_1 = 1.2$), there is an elliptic fixed point E_1 which is born along with a saddle fixed point (the latter is not presented in the phase portrait) after a parabolic bifurcation at P_1^+. At crossing P_3^+ a parabolic bifurcation of 3-periodic orbits occurs and close to the elliptic point E_1 there appear 3-periodic orbits E_3 and S_3 of elliptic and saddle type, respectively, on the right-hand side of P_3^+ (see, for example, the phase portrait ② for $M_1 = 0.98$). On the 1:3 resonance curve $l_{1:3}$, the saddle 3-periodic orbit S_3 collides with the elliptic point E_1 and they become the saddle fixed point $P_{1:3}^{(1)}$ with 6 separatrices (see the phase portrait ③ for $M_1 \approx 0.915$). After this bifurcation, the saddle 3-periodic orbit S_3 is reconstructed, and the homoclinic connections are transformed into heteroclinic cycles (see the phase portrait ④ for $M_1 = 0.83$). When passing through the left curve PF_3^+ the elliptic 3-periodic orbit E_3 undergoes a supercritical pitchfork bifurcation: it becomes a saddle $\hat{S}_3$ and a pair of nonsymmetric elliptic 3-periodic orbits $\hat{E}_3^1$ and $\hat{E}_3^2$ appears nearby (see, for instance, the phase portrait ⑤ for $M_1 = 0.03$). Then the elliptic orbits $\hat{E}_3^1$ and $\hat{E}_3^2$ move away from $\hat{S}_3$ and get closer to S_3. At the same time, the separatrices of the interior saddle $\hat{S}_3$ increase until they connect with the separatrices of the exterior saddle S_3 (the phenomenon of splitting of separatrices takes place). After some bifurcation related with homo/heteroclinic connections (phase portrait ⑥ at $M_1 = 0$) the saddle and elliptic 3-periodic orbits are rotated. Afterwards, by the symmetry in the (M_1, M_2)-plane, for $M_1 > 0$, the periodic orbits undergo an inverse pitchfork bifurcation (the elliptic 3-periodic orbits $\hat{E}_3^1$ and $\hat{E}_3^2$ merge into the saddle orbit S_3 which becomes elliptic E_3) at PF_3^+; a 1:3 resonance bifurcation (the saddle 3-periodic orbit $\hat{S}_3$ is reconstructed after passing through the saddle fixed point $P_{1:3}^{(2)}$ with 6 separatrices) takes place at $l_{1:3}^+$; an inverse parabolic

bifurcation (the saddle and elliptic 3-periodic orbits E_3 and $\hat{S}_3$ merge into the elliptic fixed point E_1) occurs at crossing P_3^+.

In Fig. 4 one can observe the bifurcations which occur when the curves $l_{1:3}^-$, P_3^- and PF_3^- are crossed, in the case of map H_3^-. We consider the horizontal line $M_2 = -0.8$. For M_1 on the right-hand side of P_3^- (see, for example, the phase portrait ① for $M_1 = 1.2$), there are an elliptic fixed point E_1 and a saddle 2-periodic orbit (the latter is absent in the figure) which appear after a period-doubling bifurcation at PD_1^-. Decreasing M_1 and passing through the curve P_3^-, elliptic and saddle 3-periodic orbits E_3 and S_3 show up, surrounding the elliptic fixed point E_1 (see, for instance, the phase portrait ② for $M_2 = 0.85$). Further, for M_1 in the curve $l_{1:3}^-$ the elliptic point E_1 and the saddle orbit S_3 are transformed into the saddle point $P_{1:3}^{(1)}$ with 6 separatrices (see the phase portrait ③ at $M_1 \approx 0.74245$), and after crossing $L_{1:3}^-$ the saddle 3-periodic orbit S_3 is rotated, reconstructing the homoclinic configuration into the heteroclinic connections (see the phase portrait ④ for $M_1 = 0.04$). After that, when crossing the right branch of PF_3^-, the saddle 3-periodic orbit S_3 goes through a subcritical pitchfork bifurcation: the saddle orbit becomes elliptic $\hat{E}_3$ and in its neighborhood there appear two nonsymmetric saddle 3-periodic orbits $\hat{S}_3^1$ and $\hat{S}_3^2$ (as in the phase portrait ⑤ at $M_1 = 0.025$). Varying further M_1, the nonsymmetric saddle orbits $\hat{S}_3^1$ and $\hat{S}_3^2$ move away from the elliptic orbit $\hat{E}_3$ toward the other elliptic orbit E_3 (see, for instance, the phase portrait ⑥ for $M_1 = 0$). For $M_1 < 0$, the two saddle orbits $\hat{S}_3^1$ and $\hat{S}_3^2$ get closer to E_3. These three orbits undergo an inverse pitchfork bifurcation while crossing the left branch of PF_3^-: the two saddle and elliptic 3-periodic orbits $\hat{S}_3^1$, $\hat{S}_3^2$ and $\hat{E}_3$ collide into the saddle 3-periodic orbit S_3. When the left branch of $l_{1:3}^-$ is crossed, the rotation of the saddle 3-periodic orbit S_3 takes place. Finally, for the parameters in the curve P_3^- the 3-periodic orbits $\hat{E}_3$ and S_3 disappear and the elliptic fixed point E_1 remains.

Remark 2. The phase portraits in Figs. 3 and 4 for values of parameters (M_1, M_2) and $(-M_1, M_2)$ are centrally symmetric with respect to the origin $x = y = 0$. This is due to the fact that the maps (1.1) are invariant under the change $x \to -x, y \to -y, M_1 \to -M_1$. This also results in the symmetries of the bifurcation curves in the (M_1, M_2) parameter plane with respect to $M_1 = 0$.

Remark 3. In Figs. 3 and 4, the saddle separatrices are shown to coincide for simplicity, although they are not expected to be exactly merged since the phenomenon of splitting of separatrices occurs (see, for instance, [41, 42] and references therein for more details about this phenomenon).

4. ON THE DEGENERACY OF THE $p : q$ RESONANCES WITH ODD $q > 3$ IN $H_3^{\pm}$ WITH $M_1 = 0$

Let us consider the conservative cubic Hénon maps with $M_1 = 0$. Due to Remark 2, there is central symmetry in the phase portraits $x \to -x, y \to -y$. A normal form for the $p : q$ resonance, where p and q are mutually prime and $q > 3$ is odd, is as follows:

$$\bar{z} = e^{i2\pi p/q}(z + \Omega(|z|^2)z^* + A(z^*)^{q-1} + Bz^{q+1} + Cz(z^*)^q).$$

The corresponding flow normal form in this case can be written as follows:

$$\dot{z} = iz + \Omega(|z|^2)z^* + A(z^*)^{q-1} + Bz^{q+1} + Cz(z^*)^q. \tag{4.1}$$

It is conservative and reversible with respect to the involution $(t, z) \to (-t, z^*)$. Applying the involution gives

$$-\dot{z}^* = iz^* + \Omega(|z|^2)z + A(z)^{q-1} + B(z^*)^{q+1} + Cz^*(z)^q.$$

Further, let us consider the complex conjugate system

$$-\dot{z} = -iz + \Omega^*(|z|^2)z^* + A^*(z^*)^{q-1} + B^*(z)^{q+1} + C^*z(z^*)^q.$$

Thus, the reversibility implies that $\Omega = -\Omega^*, A = -A^*, B = -B^*, C = -C^*$, i. e., all coefficients in (4.1) should be purely imaginary. Therefore, Eq. (4.1) takes the form

$$\dot{z} = iz + i\Omega(|z|^2)z^* + iA(z^*)^{q-1} + iBz^{q+1} + iCz(z^*)^q, \tag{4.2}$$

where all coefficients Ω, A, B, C are real. The conservativity condition means zero divergence, i.e.,

$$\frac{\partial \dot{z}}{\partial z} + \frac{\partial \dot{z}^*}{\partial z^*} \equiv 0.$$

As it follows from (4.2),

$$\frac{\partial \dot{z}}{\partial z} = i + i\Omega'(z^*)^2 + i(q+1)Bz^q + iC(z^*)^q$$

and

$$\frac{\partial \dot{z}^*}{\partial z^*} = -i - i\Omega'(z)^2 - i(q+1)B(z^*)^q - iC(z)^q.$$

Thus, the conservativity condition is

$$C + B(q+1) = 0.$$

The symmetry $z \to -z$ implies $A = B = C = 0$ since q is odd. Thus, the above condition is automatically fulfilled, and the following result holds.

Lemma 2. *For maps $H_3^{\pm}$ with $M_1 = 0$, any $p : q$ resonance at the fixed point $O(0,0)$, where $q > 3$ is odd, is at least triple degenerate.*

In Fig. 5 we illustrate this result for both cubic Hénon maps $H_3^{\pm}$. In Figs. 5a, 5b we show phase portraits near the degenerated 1:5 and 1:7 resonances for map H_3^+. These resonances occur at $M_2 \approx 0.575$ and $M_2 \approx 1.15$, respectively. As a result, four periodic orbits emerge: a pair of symmetric periodic saddles (colored in light and dark green, respectively) and a pair of nonsymmetric periodic elliptic orbits (colored in grey and black, respectively). In Figs. 5c, 5d we demonstrate phase portraits for map H_3^-. In contrast to the previous case, here periodic elliptic orbits are symmetric, while periodic saddles are nonsymmetric. Here the 1:5 resonance occurs at $M_2 \approx 0.66$ and the 1:7 resonance takes place at $M_2 \approx 1.36$.

5. ON THE 1:3 RESONANCE IN MAP $\tilde{H}_3^+(\varepsilon)$

In this section we describe symmetry-breaking bifurcations near the 1:3 resonance in $\tilde{H}_3^+(\varepsilon)$ in the form (2.4).

We apply reversible nonconservative perturbations to the conservative map H_3^+ and study their impact on the structure of the 1:3 resonance. We display the bifurcation diagram for the fixed perturbation parameter $\varepsilon = 0.05$ in Fig. 6. In comparison to the unperturbed case, we can see the slightly changed bifurcation curves $l_{1:3}^+$, P_3^+ and PF_3^+, related to the 1:3 resonance, a parabolic bifurcation of the appearance of 3-periodic orbits and a reversible pitchfork bifurcation of 3-periodic orbits, respectively. Unlike the conservative case, the bifurcation curves are not symmetric since the invariance of the map with respect to the change $M_1 \to -M_1$ (see also Remark 2) is not conserved anymore when the perturbation is added. However, the symmetry in the phase portraits with respect to the straight line $y = x$ is preserved due to the reversibility. Also, the curve PF_3^+ here is associated with the symmetry-breaking bifurcations which are nonconservative reversible pitchforks.

Let us describe the sequence of bifurcations which occur for the fixed parameter $M_2 = -1.25$ and the decreasing parameter M_1 in Fig. 6. To the right of the curve P_3^+ (see, for example, the phase portrait ① at $M_1 = 1.2$), map $\tilde{H}_3^+(\varepsilon)$ has an elliptic fixed point E_1. When P_3^+ is crossed, there appear a symmetric elliptic 3-periodic orbit E_3 and a symmetric saddle 3-periodic orbit S_3 with homoclinic loops (see the phase portrait ② for the parameter value $M_1 = 0.96$). Then, on approaching the curve $l_{1:3}^+$, the orbits S_3 and E_1 merge into a saddle fixed point with 6 separatrices

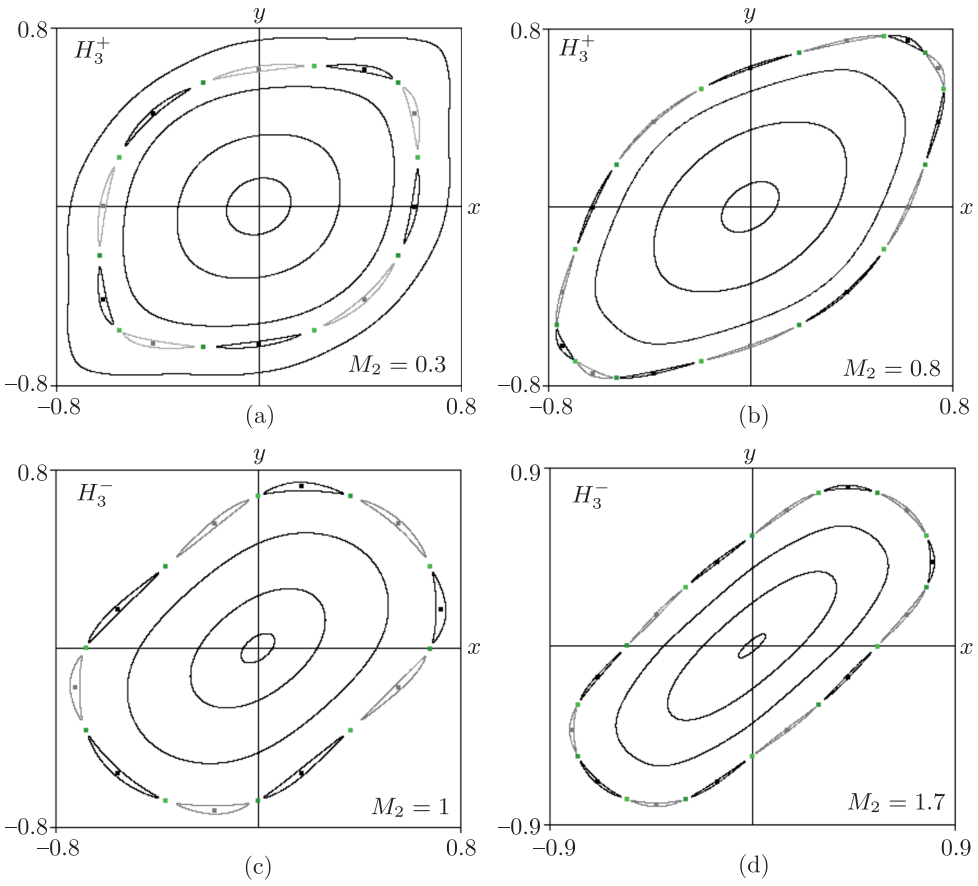

Fig. 5. Phase portraits near the degenerated 1:5 (left column) and 1:7 (right column) resonances in the conservative cubic Hénon maps H_3^+ (top row) and H_3^- (bottom row).

(the phase portrait ③ at $M_1 \approx 0.882737$). After that the saddle splits into the elliptic point E_1 and the saddle 3-periodic orbit S_3, now S_3 is rotated and forms heteroclinic connections (phase portrait ④ for $M_1 = 0.15$). Further, the elliptic 3-periodic orbit E_3 undergoes a reversible pitchfork bifurcation when crossing the right branch of the curve PF_3^+: the elliptic 3-periodic orbit E_3 breaks into saddle, stable and unstable 3-periodic orbits $\hat{S}_3$, $\hat{A}_3$ and $\hat{R}_3$, respectively (phase portrait ⑤ for $M_1 = 0.08$). Note that under this bifurcation a pair of nonsymmetric 3-periodic orbits $\hat{A}_3$ and $\hat{R}_3$ is born. The separatrices of each component of the new saddle $\hat{S}_3$ tend to the corresponding components of the stable and unstable orbits $\hat{A}_3$ and $\hat{R}_3$ at forward and backward iterations, respectively, forming homoclinic loops, and all the three components are surrounded by invariant curves in a similar way as in Fig. 1a. As M_1 decreases, the stable and unstable orbits $\hat{A}_3$ and $\hat{R}_3$ move away from each other. Moreover, one of the components of the stable (or unstable) 3-periodic orbit gets away from the symmetry line $y = x$, while the other two components move closer to each other and to the line $y = x$. At the same time, the separatrices of the inner saddles become larger. At some instant (close to $M_1 = 0.055$, see the phase portrait ⑥), the separatrices of the inner and exterior saddles $\hat{S}_3$ and S_3 merge (not exactly due to splitting of separatrices) and the transformation of homoclinic/heteroclinic connections takes place, after which all the involved 3-periodic orbits are rotated (as in the phase portrait ⑦ for $M_1 = 0.03$). When the left branch of PF_3^+ is crossed, an inverse pitchfork bifurcation occurs: the saddle, stable and unstable 3-periodic orbits S_3, $\hat{A}_3$ and $\hat{R}_3$ merge into an elliptic 3-periodic orbit E_3 (phase portrait ⑧ at $M_1 = 0$). The remaining saddle 3-periodic orbit $\hat{S}_3$ and the elliptic point E_1 collide on crossing the left branch of $l_{1:3}^+$, there is a saddle point with 6 separatrices for the parameters in this curve (for a parameter close to $M_1 = -0.95$, see the phase portrait ⑨). After the bifurcation, the 6-separatrix saddle splits

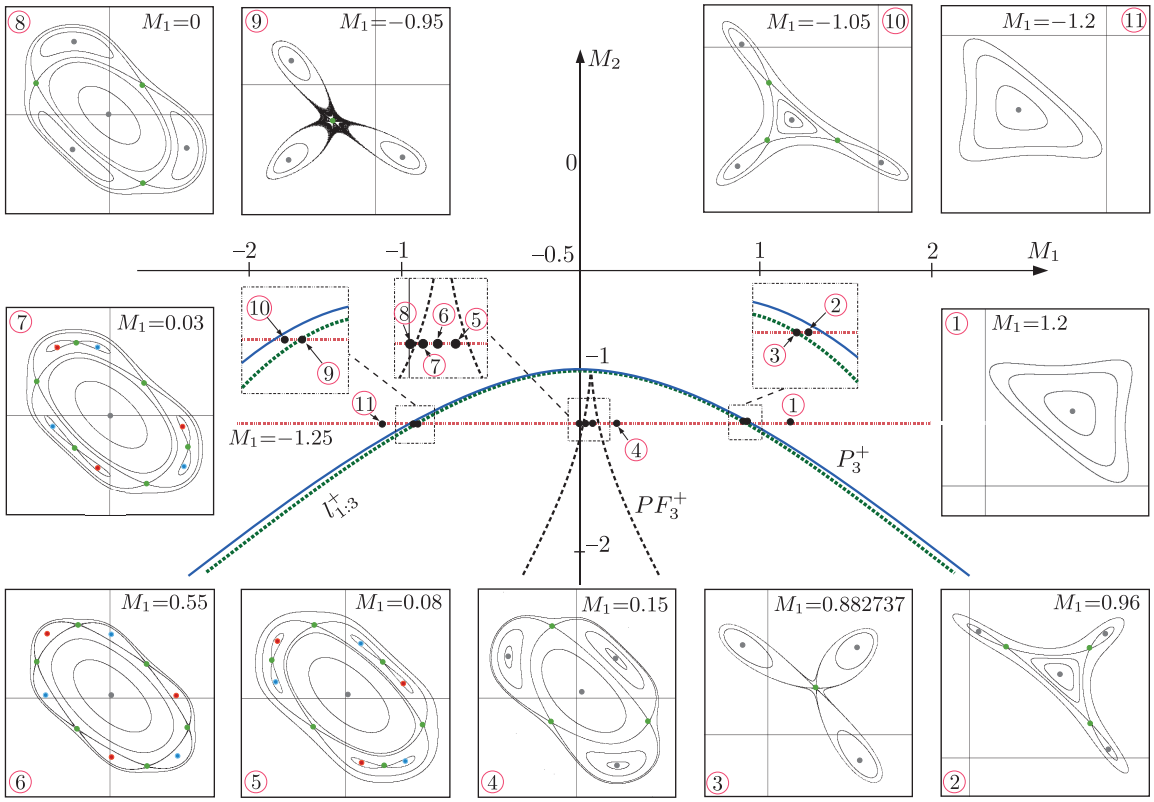

Fig. 6. Bifurcation diagram for the reversible nonconservative map $\tilde{H}_3^+(\varepsilon)$ for $\varepsilon = 0.05$ near the 1:3 resonance. The bifurcations curve $l_{1:3}^+$ is the curve of the 1:3 resonance of fixed points, while the curves P_3^+ and PF_3^+ are related to parabolic and reversible pitchforks (nonconservative symmetry-breaking) bifurcations of 3-periodic orbits, respectively. For the fixed value of $M_2 = -1.25$, the phase portraits are given for $M_1 = -1.2, -1.05, -.0.95, 0, 0.003, 0.055, 0.08, 0.15, 0.8827, 0.96$, and 1.2. Green, grey, red and blue stand for saddle, elliptic, stable (sinks) and unstable (sources) fixed points and periodic orbits, respectively.

into saddle and elliptic 3-periodic orbits $\hat{S}_3$ and E_3 on the left-hand side of $l_{1:3}^+$, now $\hat{S}_3$ is rotated by $\pi/3$ and the heteroclinic cycles change into homoclinic loops (phase portrait ⑩ for $M_1 = -1.05$). Finally, we transit the curve P_3^+ and the 3-periodic orbits $\hat{S}_3$ and E_3 disappear (phase portrait ⑪ for $M_1 = -1.2$).

Thus, during transition into the domain lying below the curve PF_3^+, there appears a symmetric pair of nonsymmetric stable and completely unstable 3-periodic orbits. This fact is relevant for detecting mixed dynamics in maps with symmetric cubic homoclinic tangencies whose truncated first return map is $\tilde{H}_3^+(\varepsilon)$. Thus, there are Newhouse domains where maps with infinitely many attracting, repelling, saddle and elliptic periodic orbits are dense [18, 19, 21, 43].

6. ON THE 1:3 RESONANCE IN MAP $\tilde{H}_3^-(\varepsilon)$

In this section we study how the 1:3 resonance evolves under the perturbation in the case of map $\tilde{H}_3^-(\varepsilon)$. The corresponding bifurcation diagram is illustrated in Fig. 7. Unlike the unperturbed case in Fig. 4, the 1:3 resonance curve $l_{1:3}^-$ as well as the curves P_3^- and PF_3^- related to parabolic and reversible pitchfork bifurcations of 3-periodic orbits, respectively, are nonsymmetric and slightly moved, since the symmetry with respect to $M_1 = 0$ (see also Remark 2) is not conserved anymore. Also, PF_3^- corresponds to a nonconservative symmetry-breaking bifurcation, after which two nonsymmetric saddle 3-periodic orbits appear, one of them with the Jacobian $J > 1$ and the other with the Jacobian $J < 1$.

Let us give details on the bifurcations taking place in the bifurcation diagrams in Fig. 7. We choose the horizontal line $M_2 = -0.8$. We start with the parameters on the right-hand side of P_3^-

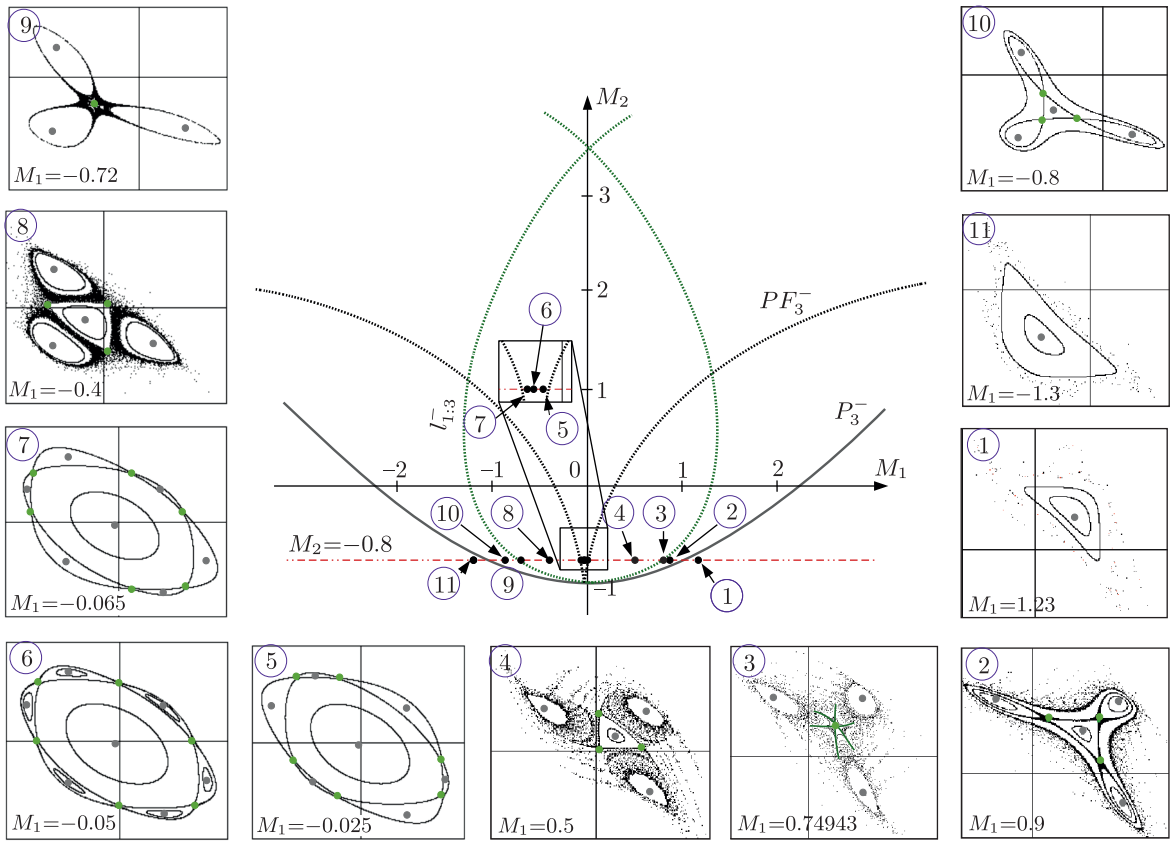

Fig. 7. Bifurcation diagram for the reversible nonconservative map $\tilde{H}_3^-(\varepsilon)$ for $\varepsilon = 0.05$ near the 1:3 resonance. The bifurcations curve $l_{1:3}^-$ is related to bifurcations of the 1:3 resonance of fixed points, while the curves P_3^- and PF_3^- correspond to parabolic and reversible pitchfork (nonconservative symmetry-breaking) bifurcations of 3-periodic orbits, respectively. For the fixed value of $M_2 = -0.8$, the phase portraits are given for $M_1 = -1.3, -0.8, -0.72, -0.4, -0.065, -0.005, -0.025, 0.5, 0.7494, 0.9$ and 1.23. The green and grey points stand for saddle and elliptic orbits, respectively.

(see, for instance, the phase portrait ① for $M_1 = 1.23$), where map $\tilde{H}_3^-(\varepsilon)$ has an elliptic fixed point E_1. The point E_1 undergoes a parabolic bifurcation when crossing P_3^- and there appear 3-periodic orbits S_3 and E_3 of saddle and elliptic type close to E_1 for the parameters on the left-hand side of P_3^- (phase portrait ② for $M_1 = 0.9$). Note that the three components of the saddle orbit S_3 have homoclinic loops. On the 1:3 resonance curve $l_{1:3}^-$ (at $M_1 \approx 0.74943$), the saddle 3-periodic orbit S_3 and the elliptic point E_1 merge into a saddle fixed point with 6 separatrices (see the phase portrait ③) which for the parameters on the left-hand side of $l_{1:3}^-$ breaks into saddle and elliptic 3-periodic orbits S_3 and E_3 again, but on the left-hand side of $l_{1:3}^-$ the orbit S_3 is rotated by $\pi/3$ and the homoclinic loops of S_3 are reorganized into heteroclinic connections (see, for example, the phase portrait ④ at $M_1 = 0.5$). When crossing the right branch of the curve PF_3^-, the saddle orbit S_3 undergoes the subcritical pitchfork bifurcation. As a result, the saddle orbit is converted into an elliptic 3-periodic orbit $\hat{E}_3$ and two saddle 3-periodic orbits $\hat{S}_3^1$ and $\hat{S}_3^2$ show up nearby (see the phase portrait ⑤ for $M_1 = -0.025$). Moreover, the Jacobian in $\hat{S}_3^1$ is greater than 1 and the Jacobian in $\hat{S}_3^2$ is less than 1. As the parameter M_1 decreases, the saddle orbits $\hat{S}_3^1$ and $\hat{S}_3^2$ move away from each other toward the elliptic orbit E_3 (phase portraits ⑥ and ⑦ for $M_1 = -0.05$ and $M_1 = -0.065$). In the left branch of PF_3^-, an inverse pitchfork bifurcation takes place: the orbit E_3 merges along with $\hat{S}_3^1$ and $\hat{S}_3^2$ into a saddle 3-periodic orbit S_3 (phase portrait ⑧ for $M_1 = -0.4$). Afterwards, the reconstruction of S_3 happens on the 1:3 resonance curve $l_{1:3}^-$ (phase

portrait ⑨ and ⑩ for $M_1 = -0.72$ and $M_1 = -0.8$). Finally, the 3-periodic orbits $\hat{E}_3$ and S_3 disappear on crossing P_3^- (phase portrait ⑪) for $M_1 = -1.3$).

Note that in the domain above the curve PF_3^- there emerges a symmetric pair of nonsymmetric saddle 3-periodic orbits whose Jacobians are greater and less than 1. This configuration also implies the existence of mixed dynamics in maps with cubic homoclinic tangencies whose truncated first return map is $\tilde{H}_3^-(\varepsilon)$. Also in $\tilde{H}_3^-(\varepsilon)$ itself we show numerically the existence of mixed dynamics for the parameters from the domain inside PF_3^- since heteroclinic connections between two saddle orbits, one with the Jacobian $J > 1$ and the other with the Jacobian $J < 1$, leads to the presence of nontransversal heteroclinic cycles [19]. See Section 7 for more details.

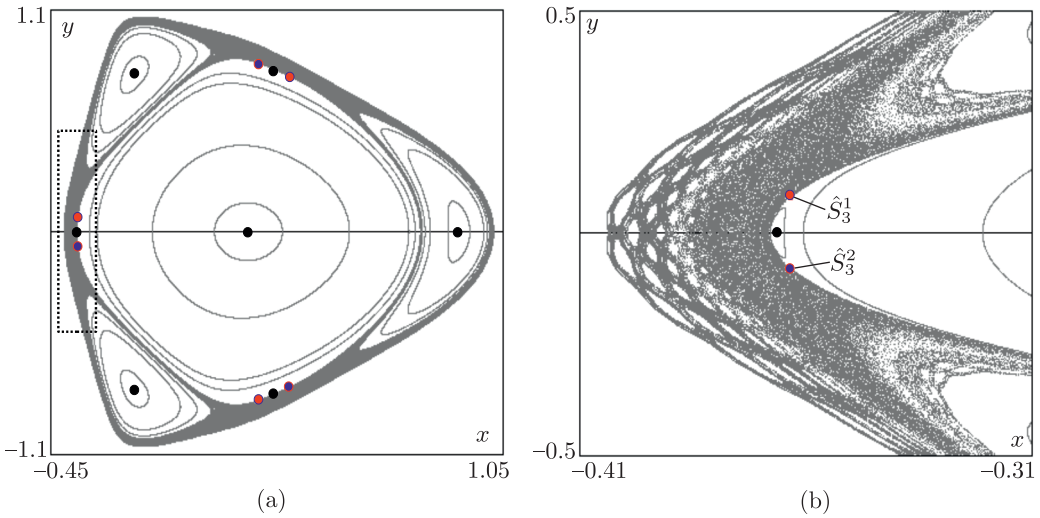

Fig. 8. Phase portrait and the zoomed fragment for map $\tilde{H}_3^-(\varepsilon)$ in (2.4) for $M_1 = -0.364, M_2 = -0.5$ and $\varepsilon = 0.3$. For convenience, the phase portrait is rotated by $\pi/4$. In this representation, the horizontal axis becomes $Fix(h)$. The chaotic dynamics (in the gray region) seems conservative (the phase portrait is self-symmetric with respect to the horizontal axis). The orbits $\hat{S}_3^1$ and $\hat{S}_3^2$ are the pair of nonconservative saddle 3-periodic orbits with the Jacobians $J(\hat{S}_3^1) = 0.995 < 1$ and $J(\hat{S}_3^2) = 1.005 > 1$.

7. NUMERICAL EVIDENCE OF MIXED DYNAMICS IN THE PERTURBED MAP $\tilde{H}_3^-(\varepsilon)$

In this section we provide numerical evidence of the existence of mixed dynamics in the perturbed map $\tilde{H}_3^-(\varepsilon)$ in (2.4) for which in Section 6 we show the existence of a pair of saddle 3-periodic orbits $\hat{S}_3^1$ and $\hat{S}_3^2$ with the Jacobians $J < 1$ and $J > 1$, respectively. Recall that these orbits appear due to a subcritical reversible pitchfork bifurcation of the symmetric saddle 3-periodic orbit S_3. For better visibility, we take a quite large value of perturbation, $\varepsilon = 0.3$. In Fig. 8 we show the phase portraits of $\tilde{H}_3^-(\varepsilon)$ for $M_1 = -0.364$ and $M_2 = -0.5$. The orbits $\hat{S}_3^1$ with $J < 1$, $\hat{S}_3^2$ with $J > 1$ and symmetric elliptic orbits are marked by blue, red and black bold points, respectively. For convenience, we rotate the phase portraits by $\pi/4$, then the horizontal axis corresponds to $Fix(h)$.

From Fig. 8 it is clearly seen that the phase portrait is self-symmetric with respect to the horizontal axis, which means that the attractor of the system seems coincident with the repeller. Moreover, we are not able to find periodic sinks and sources nor even nonsymmetric orbits (except for points $\hat{S}_3^1$ and $\hat{S}_3^2$) which would confirm mixed dynamics in $\tilde{H}_3^-(\varepsilon)$.[3)]

However, we find a nontransversal heteroclinic cycle [19] which connects $\hat{S}_3^1$ and $\hat{S}_3^2$. As it was shown in [19], bifurcations of such cycles lead to reversible mixed dynamics. A schematic

[3)] Everywhere in numerical experiments, we use double-precision numbers. The use of multiple-precision packages for the detection of periodic sinks and sources with extremely small absorbing domains seems to be a challenging, but important problem for future studies.

representation of this cycle is shown in Fig. 9a. The numerically obtained cycle is presented in Fig. 9b. From this figure, one can see that the stable and unstable manifolds of $\hat{S}_3^1$ and $\hat{S}_3^2$ have both transversal (see also the zoomed region near $\hat{S}_3^2$ in Fig. 9c) and nontransversal (see the zoomed fragment in Fig. 9b) intersections. Thus, we can state that the chaotic dynamics presented in the gray zone in Fig. 8 is mixed.

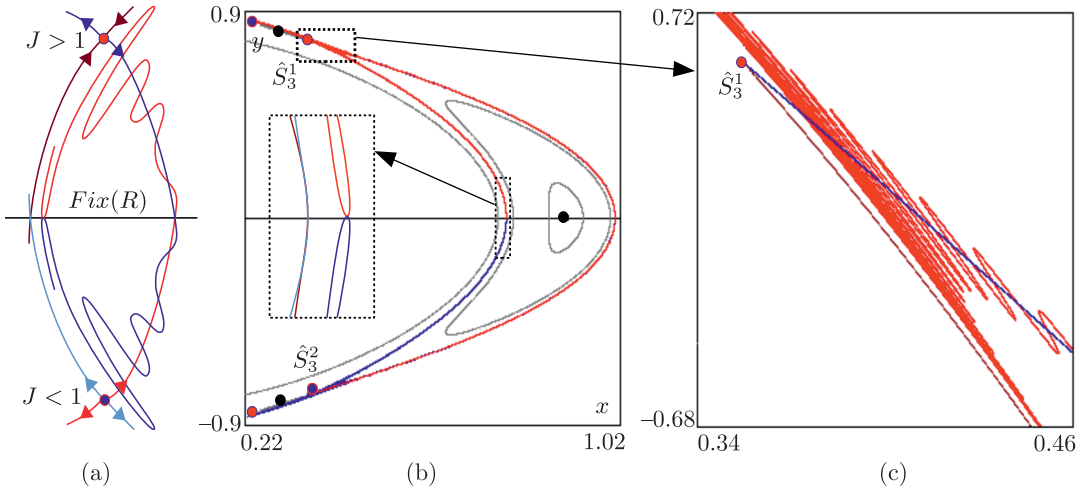

Fig. 9. (a) A schematic representation of the nontransversal heteroclinic cycle. (b), (c) Nontransversal heteroclinic cycle connecting saddles $\hat{S}_3^1$ and $\hat{S}_3^2$ in map $\tilde{H}_3^-(\varepsilon)$ at $M_1 = -0.364, M_2 = -0.5$ and $\varepsilon = 0.3$. A pair of manifolds W_1^s and W_1^u intersects transversally, while the other pair W_2^s and W_2^u has a quadratic tangency.

Also in this section we would like to note that the presence of mixed dynamics near elliptic points of two-dimensional reversible maps plays an important role. As is well known, the phase portrait near an elliptic point of a two-dimensional reversible diffeomorphism is organized in many details as in the conservative case. There is also a continuum of KAM-curves surrounding the elliptic point. The KAM-curves are separated by resonant zones [44]. However, the behavior in the resonant zones for reversible maps differs greatly from the conservative ones, compare, for example, Figs. 10a and 10b. In the conservative setting, ε-orbits can run away from any neighborhood of an elliptic point, i.e., such a point is not stable under permanently acting perturbations (Lyapunov instability by ε-orbits) [3], see Fig. 10a.

On the other hand, in the reversible nonconservative case, as it follows from [3, 32], it is typical when in resonant zones periodic saddle points alternate with symmetric pairs of sinks and sources, see Fig. 10b. In this case, it is possible when there exist intersecting absorbing domain B_A and repelling domain B_R around an elliptic point such that forward as well as backward ε-orbits of any point that belongs to the intersection $B_A \cap B_R$, cannot leave any neighborhood of this elliptic point [3, 17]. These resonances are called *impassable* or *isolated*. We could not find such resonances in the maps under consideration. However, we believe that by varying a perturbation and parameters of the maps one can find them in numerical experiments. In future papers, we plan to study such impassable resonances for the perturbed reversible nonconservative Hénon maps.

CONCLUSIONS

In the present paper we have obtained a series of new results devoted to the structure of the 1:3 resonance in the conservative cubic Hénon maps and their reversible perturbations. First, we have proposed the method which gives reversible nonconservative perturbations of the conservative cubic Hénon maps. We have proved that the resulting perturbed perturbations preserve reversibility. Second, we have considered the conservative cubic Hénon maps H_3^+ and H_3^- as examples and studied the influence of reversible nonconservative perturbations on the structure of bifurcations of the 1:3 resonance. We have provided a detailed analysis of these bifurcations in the perturbed

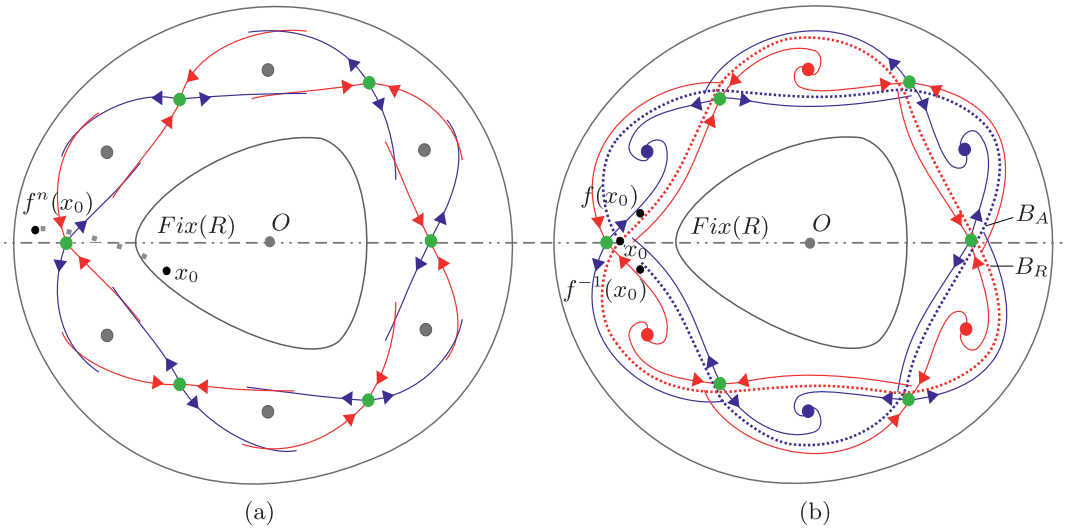

Fig. 10. Different types of behavior in resonant zones of a symmetric elliptic point in the conservative (a) and reversible (b) cases. Periodic elliptic orbits are marked by gray bold points, while periodic sinks and sources are colored in blue and red, respectively. In plot (b) the absorbing domain B_A of a sink orbit (bounded by the blue dashed curves) intersects with the repelling domain of the source orbit (bounded by the red dashed curves). Thus, ε-orbits of any point belonging to this intersection cannot leave the resonant zone, with either forward or backward iterations (isolated resonance). This means that an elliptic point of a typical two-dimensional reversible diffeomorphism is stable under permanently acting perturbations (Lyapunov stability by ε-orbits).

maps. We have focused on local symmetry-breaking bifurcations which have led to the appearance of nonsymmetric orbits. These bifurcations are reversible pitchfork bifurcations of 3-periodic orbits, and we have found the domains of parameters corresponding to nonsymmetric orbits. Moreover, for perturbations of H_3^+, there appear nonsymmetric asymptotically stable and completely unstable 3-periodic orbits, while in perturbed H_3^- there emerge two nonsymmetric saddle 3-periodic orbits, one with the Jacobian greater than 1 and the other with the Jacobian less than 1. The presence of these nonsymmetric orbits leads to the existence of mixed dynamics in maps with cubic homoclinic tangencies whose first return maps are $H_3^\pm$. Third, for the unperturbed conservative maps H_3^+ and H_3^- with $M_1 = 0$, we have demonstrated that all $p : q$ resonances are degenerate when $q > 3$ is odd. And finally, we have provided numerical evidence of mixed dynamics in perturbed H_3^-, since a heteroclinic configuration between these nonsymmetric saddle orbits implies the emergence of nontransversal heteroclinic cycles.

These results can be used for further study of mechanisms of the appearance of mixed dynamics after a break-down of conservative dynamics. As pointed out in the Introduction, maps (1.1) are related to the study of cubic homoclinic tangencies and the phenomenon of mixed dynamics, the third (and the last) type of chaos. We have shown some global and local mechanisms of its emergence. The global ones are connected with the presence of homoclinic and heteroclinic cycles of different kinds, while one of the interesting local mechanisms is related to bifurcations of resonances among which we highlight the 1:3 resonance. It is easy to associate the bifurcation structure of cubic Hénon maps with the bifurcations which take place near cubic homoclinic tangencies [26]. In the present paper we have proposed a local mechanism corresponding to the occurrence of degenerate resonances in cubic Hénon maps. In the reversible context, symmetry-breaking pitchfork bifurcations of 3-periodic orbits lead to the appearance of pairs of nonsymmetric and nonconservative periodic orbits (periodic sinks and sources, periodic saddles with the Jacobians greater and less than 1) near the degenerate 1:3 resonant point. In this regard, we think that it is of great importance to consider the problem of local 1:3 resonance, especially the degeneracy $a_{02} = 0$ in (3.1), and the accompanying symmetry-breaking bifurcations in general reversible maps, since degenerate resonances in reversible systems are the main local mechanism of the appearance of mixed dynamics. It is also worth mentioning that the similar problem for the 1:4 resonance, the structure of bifurcations associated with fixed points with eigenvalues $e^{\pm\pi/2} = \pm i$ and, consequently,

4-periodic orbits, is of great interest as well. An exhaustive study of 1:4 resonance for (1.1) was done in [26, 31], see also [45]. It was also established in these works that, for some (M_1, M_2), the 1:4 resonance can be degenerate and the 4-periodic orbits are subject to pitchfork bifurcations. The study of reversible nonconservative perturbations for this case is planned in a forthcoming paper.

ACKNOWLEDGMENTS

The authors thank S. V. Gonchenko, D. Turaev, and K. Safonov for fruitful discussions.

FUNDING

This paper was supported by the RSF grant No. 19-71-10048. Numerical experiments described in Section 7 were supported by the Laboratory of Dynamical Systems and Applications NRU HSE, of the Russian Ministry of Science and Higher Education (Grant No. 075-15-2019-1931). The work presented in Section 3 was supported by the RSF grant No. 19-11-00280. M. Gonchenko is partially supported by Juan de la Cierva-Incorporación fellowship IJCI-2016-29071 and the Spanish grant PGC2018-098676-B-I00 (AEI/FEDER/UE). A. Kazakov and E. Samylina also acknowledge the Theoretical Physics and Mathematics Advancement Foundation BASIS for financial support of scientific investigations.

CONFLICT OF INTEREST

The authors declare that they have no conflicts of interest.

REFERENCES

1. Dullin, H. R. and Meiss, J. D., Generalized Hénon Maps: The Cubic Diffeomorphisms of the Plane. Bifurcations, Patterns and Symmetry, *Phys. D,* 2000, vol. 143, nos. 1–4, pp. 262–289.
2. Gonchenko, S. V., Reversible Mixed Dynamics: A Concept and Examples, *Discontinuity Nonlinearity Complex.,* 2016, vol. 5, no. 4, pp. 365–374.
3. Gonchenko, S. V. and Turaev, D. V., On Three Types of Dynamics and the Notion of Attractor, *Proc. Steklov Inst. Math.,* 2017, vol. 297, no. 1, pp. 116–137; see also: *Tr. Mat. Inst. Steklova,* 2017, vol. 297, pp. 133–157.
4. Gonchenko, A. S., Gonchenko, S. V., and Kazakov, A. O., Richness of Chaotic Dynamics in the Nonholonomic Model of Celtic Stone, *Regul. Chaotic Dyn.,* 2013, vol. 18, no. 5, pp. 521–538.
5. Kazakov, A. O., Strange Attractors and Mixed Dynamics in the Unbalanced Rubber Ball on a Plane Problem, *Regul. Chaotic Dyn.,* 2013, vol. 18, no. 5, pp. 508–520.
6. Gonchenko, A. S., Gonchenko, S. V., Kazakov, A. O., and Turaev, D. V., On the Phenomenon of Mixed Dynamics in Pikovsky – Topaj System of Coupled Rotators, *Phys. D,* 2017, vol. 350, pp. 45–57.
7. Kuznetsov, S. P., Regular and Chaotic Motions of the Chaplygin Sleigh with Periodically Switched Location of Nonholonomic Constraint, *Europhys. Lett.,* 2017, vol. 118, no. 1, 10007, 10 pp.
8. Kuznetsov, S. P., Regular and Chaotic Dynamics of a Chaplygin Sleigh due to Periodic Switch of the Nonholonomic Constraint, *Regul. Chaotic Dyn.,* 2018, vol. 23, no. 2, pp. 178–192.
9. Emelianova, A. A. and Nekorkin, V. I., On the Intersection of a Chaotic Attractor and a Chaotic Repeller in the System of Two Adaptively Coupled Phase Oscillators, *Chaos,* 2019, vol. 29, no. 11, 111102, 7 pp.
10. Kazakov, A. O., On the Appearance of Mixed Dynamics As a Result of Collision of Strange Attractors and Repellers in Reversible Systems, *Radiophys. Quantum El.,* 2019, vol. 61, nos. 8–9, pp. 650–658; see also: *Izv. Vyssh. Uchebn. Zaved. Radiofizika,* 2018, vol. 61, nos. 8–9, pp. 729–738.
11. Ariel, G. and Schiff, J., Conservative, Dissipative and Super-Diffusive Behavior of a Particle Propelled in a Regular Flow, *Phys. D,* 2020, vol. 411, 132584, 9 pp.
12. Emelianova, A. A. and Nekorkin, V. I., The Third Type of Chaos in a System of Two Adaptively Coupled Phase Oscillators, *Chaos,* 2020, vol. 30, no. 5, 051105, 8 pp.
13. Bizyaev, I. A. and Mamaev, I. S., Separatrix Splitting and Nonintegrability in the Nonholonomic Rolling of a Generalized Chaplygin Sphere, *Int. J. Non-Linear Mech.,* 2020, vol. 126, 103550, 7 pp.
14. Bizyaev, I. A. and Mamaev, I. S., Dynamics of the Nonholonomic Suslov Problem under Periodic Control: Unbounded Speedup and Strange Attractors, *J. Phys. A,* 2020, vol. 53, no. 18, 185701, 17 pp.

15. Emelianova, A. A. and Nekorkin, V. I., Emergence and Synchronization of a Reversible Core in a System of Forced Adaptively Coupled Kuramoto Oscillators, *Chaos,* 2021, vol. 31, no. 3, 033102, 7 pp.

16. Kuznetsov, S. P., Kruglov, V. P., and Borisov, A. V., Chaplygin Sleigh in the Quadratic Potential Field, *Europhys. Lett.,* 2020, vol. 132, no. 2, 20008, 7 pp.

17. Gonchenko, S. V., Gonchenko, A. S., and Kazakov, A. O., Three Types of Attractors and Mixed Dynamics of Nonholonomic Models of Rigid Body Motion, *Proc. Steklov Inst. Math.,* 2020, vol. 308, pp. 125–140; see also: *Tr. Mat. Inst. Steklova,* 2020, vol. 308, pp. 135–151.

18. Gonchenko, S. V., Turaev, D. V., and Shilnikov, L. P., On Newhouse Domains of Two-Dimensional Diffeomorphisms That Are Close to a Diffeomorphism with a Structurally Unstable Heteroclinic Contour, *Proc. Steklov Inst. Math.,* 1997, vol. 216, pp. 70–118; see also: *Tr. Mat. Inst. Steklova,* 1997, vol. 216, pp. 76–125.

19. Lamb, J. S. W. and Stenkin, O. V., Newhouse Regions for Reversible Systems with Infinitely Many Stable, Unstable and Elliptic Periodic Orbits, *Nonlinearity,* 2004, vol. 17, no. 4, pp. 1217–1244.

20. Delshams, A., Gonchenko, S. V., Gonchenko, A. S., Lázaro, J. T., and Sten'kin, O., Abundance of Attracting, Repelling and Elliptic Periodic Orbits in Two-Dimensional Reversible Maps, *Nonlinearity,* 2013, vol. 26, no. 1, pp. 1–33.

21. Gonchenko, S. V., Gonchenko, M. S., and Sinitsky, I. O., On Mixed Dynamics of Two-Dimensional Reversible Diffeomorphisms with Symmetric Nontransversal Heteroclinic Cycles, *Izv. Math.,* 2020, vol. 84, no. 1, pp. 23–51; see also: *Izv. Ross. Akad. Nauk Ser. Mat.,* 2020, vol. 84, no. 1, pp. 27–59.

22. Kazakov, A., Merger of a Hénon-Like Attractor with a Hénon-Like Repeller in a Model of Vortex Dynamics, *Chaos,* 2020, vol. 30, no. 1, 011105, 7 pp.

23. Chigarev, V., Kazakov, A., and Pikovsky, A., Kantorovich – Rubinstein – Wasserstein Distance between Overlapping Attractor and Repeller, *Chaos,* 2020, vol. 30, no. 7, 073114, 10 pp.

24. Turaev, D., Maps Close to Identity and Universal Maps in the Newhouse Domain, *Comm. Math. Phys.,* 2015, vol. 335, no. 3, pp. 1235–1277.

25. Newhouse, Sh. E., The Abundance of Wild Hyperbolic Sets and Nonsmooth Stable Sets for Diffeomorphisms, *Inst. Hautes Études Sci. Publ. Math.,* 1979, No. 50, pp. 101–151.

26. Gonchenko, M., Gonchenko, S., and Ovsyannikov, I., Bifurcations of Cubic Homoclinic Tangencies in Two-Dimensional Symplectic Maps, *Math. Model. Nat. Phenom.,* 2017, vol. 12, no. 1, pp. 41–61.

27. Gonchenko, S. V., On a Two Parameter Family of Systems Close to a System with a Nontransversal Poincaré Homoclinic Curve: 1, *Selecta Math. Soviet.,* 1991, vol. 10, no. 1, pp. 69–80; see also: *Differential and Integral Equations,* N. F. Otrokov (Ed.), Gorki: GGU, 1985, pp. 55–72.

28. Gonchenko, S. V., Simó, C., and Vieiro, A., Richness of Dynamics and Global Bifurcations in Systems with a Homoclinic Figure-Eight, *Nonlinearity,* 2013, vol. 26, no. 3, pp. 621–678.

29. Arnol'd, V. I., *Geometrical Methods in the Theory of Ordinary Differential Equations,* 2nd ed., Grundlehren Math. Wiss., vol. 250, New York: Springer, 1988.

30. Arnol'd, V. I., Kozlov, V. V., and Neĭshtadt, A. I., *Mathematical Aspects of Classical and Celestial Mechanics,* 3rd ed., Encyclopaedia Math. Sci., vol. 3, Berlin: Springer, 2006.

31. Gonchenko, M., Gonchenko, S. V., Ovsyannikov, I., and Vieiro, A., On Local and Global Aspects of the 1 : 4 Resonance in the Conservative Cubic Hénon Maps, *Chaos,* 2018, vol. 28, no. 4, 043123, 15 pp.

32. Gonchenko, S. V., Lèmb, Ĭ. S. V., Rios, I., and Turaev, D., Attractors and Repellers in the Neighborhood of Elliptic Points of Reversible Systems, *Dokl. Math.,* 2014, vol. 89, no. 1, pp. 65–67; see also: *Dokl. Akad. Nauk,* 2014, vol. 454, no. 4, pp. 375–378.

33. Biragov, V. S., Bifurcations in a Two-Parameter Family of Conservative Mappings That Are Close to the Hénon Mapping, *Selecta Math. Soviet.,* 1990, vol. 9, no. 3, pp. 273–282; see also: *Methods of the Qualitative Theory of Differential Equations,* Gorki: GGU, 1987, pp. 10–24.

34. Simó, C. and Vieiro, A., Resonant Zones, Inner and Outer Splittings in Generic and Low Order Resonances of Area Preserving Maps, *Nonlinearity,* 2009, vol. 22, no. 5, pp. 1191–1245.

35. Gonchenko, M. S., Gonchenko, S. V., and Safonov, K., Reversible Perturbations of Conservative Hénon-Like Maps, *Discrete Contin. Dyn. Syst.,* 2021, vol. 41, no. 4, pp. 1875–1895.

36. Lerman, L. M. and Turaev, D. V., Breakdown of Symmetry in Reversible Systems, *Regul. Chaotic Dyn.,* 2012, vol. 17, nos. 3–4, pp. 318–336.

37. Roberts, J. A. G. and Quispel, G. R. W., Chaos and Time-Reversal Symmetry: Order and Chaos in Reversible Dynamical Systems, *Phys. Rep.,* 1992, vol. 216, nos. 2–3, pp. 63–177.

38. Bessa, M., Carvalho, M., and Rodrigues, A., Generic Area-Preserving Reversible Diffeomorphisms, *Nonlinearity,* 2015, vol. 28, no. 6, pp. 1695–1720.

39. Kuznetsov, Yu. A., *Elements of Applied Bifurcation Theory,* Appl. Math. Sci., vol. 112, New York: Springer, 1995.

40. Broer, H., Hanßmann, H., Jorba, À., Villanueva, J., and Wagener, F., Normal-Internal Resonances in Quasi-Periodically Forced Oscillators: A Conservative Approach, *Nonlinearity,* 2003, vol. 16, no. 5, pp. 1751–1791.

41. Delshams, A., Gonchenko, M., and Gutiérrez, P., Exponentially Small Splitting of Separatrices and Transversality Associated to Whiskered Tori with Quadratic Frequency Ratio, *SIAM J. Appl. Dyn. Syst.,* 2016, vol. 15, no. 2, pp. 981–1024.

42. Delshams, A., Gonchenko, M., and Gutiérrez, P., Exponentially Small Splitting of Separatrices Associated to 3D Whiskered Tori with Cubic Frequencies, *Comm. Math. Phys.,* 2020, vol. 378, no. 3, pp. 1931–1976.

43. Turaev, D., Richness of Chaos in the Absolute Newhouse Domain, in *Proc. of the Internat. Congr. of Mathematicians: Vol. 3,* New Delhi: Hindustan Book Agency, 2010, pp. 1804–1815.

44. Sevryuk, M. B., *Reversible Systems,* Lecture Notes in Math., vol. 1211, Berlin: Springer, 2006.

45. Gonchenko, M. S., On the Structure of 1 : 4 Resonances in Hénon Maps, *Internat. J. Bifur. Chaos Appl. Sci. Engrg.,* 2005, vol. 15, no. 11, pp. 3653–3660.